A Novel, Layered Phase in Ti-Rich $SrTiO_3$ Epitaxial Thin Films

*Sungki Lee, Anoop R. Damodaran, Prashun Gorai, Nuri Oh, Jarrett A. Moyer, Ji-Hwan Kwon, Naheed Ferdous, Amish Shah, Zuhuang Chen, Eric Breckenfeld, R. V. K. Mangalam, Paul V. Braun, Peter Schiffer, Moonsub Shim, Jian-Min Zuo, Elif Ertekin, and Lane W. Martin**

Self-assembled oxide nanostructures produced, for example, via eutectic phase separation, spinodal decomposition-like routes, and other pathways[1–8] have drawn considerable interest for their varied properties. Such approaches leverage innate chemical and thermodynamic driving forces that favor the spontaneous separation of two phases into an equilibrium state characterized by potentially complex micro- and nanostructures (i.e., layered structures, vertically aligned rods in a matrix, etc.) and exotic composite properties.[4,7,9] Researchers have demonstrated the ability to control the geometry, shape, and size of such phase-separated structures by tuning material composition,[10] growth temperature,[11] strain state,[12] growth, and cooling rates.[3,13–17] Deterministic and ordered materials self-assembly in these systems is, however, a challenge. In particular, it is difficult to access submicron feature sizes in eutectic systems due to the high processing temperatures and fast cooling rates that must be used.[1–4] Although spinodal decomposition-like routes have been used to produce nanoscale features, producing long-range ordered arrays of features via this approach is difficult.[10]

On the other hand, non-equilibrium approaches, including modern thin-film growth techniques, can be applied to systems to produce atomically and chemically precise artificial heterostructures and nanostructures.[18,19] Leveraging advances in deposition techniques and the development of in situ characterization methods, these approaches push the edge of materials control. Using these techniques it is possible to produce exotic new phases that do not exist in the bulk,[20,21] synthesize artificial heterostructures,[22,23] and control materials at the unit-cell level to enable new states of matter.[24,25] Although these approaches provide unprecedented control, they are limited in the geometries of phases that can be created (i.e., layered heterostructures) and the cost, complexity, and lack of scalability of the continuous in situ monitoring makes large scale use challenging.

In this work, we explore a new, self-assembly route to produce novel phases, whereby we combine systems with a tendency for spontaneous phase separation with non-equilibrium deposition techniques and thin-film epitaxy. The goal is to explore the evolution of a classical equilibrium concept (i.e., eutectic materials) under non-equilibrium growth conditions that are kinetically limited and influenced by epitaxial relationships. To do this, we focus on a model oxide eutectic system: $SrTiO_3$–TiO_2. The equilibrium $SrTiO_3$–TiO_2 eutectic phase diagram has been known for decades,[26] but this work is motivated by a number of recent studies. First, directional solidification of this eutectic system has produced exotic, split-ring resonator-like TiO_2 features embedded in a $SrTiO_3$ matrix.[16] Second is the use of complex shuttered thin-film deposition processes and epitaxy to study new members of the $Sr_{n+1}Ti_nO_{3n+1}$ Ruddlesden–Popper (RP) homologous series and their properties.[27,28] It should be noted that most work on the Ti-rich side of the phase diagram has been done in the context of bulk eutectic systems and what little work has been done on the Ti-rich materials as films has shown only the production of amorphous TiO_x inclusions in a $SrTiO_3$ matrix.[29] Most thin-film work in this system has focused on nearly stoichiometric $SrTiO_3$ or Sr-excess phases. This begs the question of whether non-equilibrium growth techniques and thin-film epitaxy can be used to produce novel phases and/or nanostructures akin to those observed in Sr-rich $SrTiO_3$ on the Ti-rich side of the phase diagram. Here, we study the growth, structure, and properties of the Ti-rich portion of the $SrTiO_3$–TiO_2 phase diagram in and around the eutectic composition. We observe that the non-equilibrium nature of the growth process results in films that greatly exceed the thermodynamic solubility limit of Ti in $SrTiO_3$ (≈0.5 mol% of Ti in bulk $SrTiO_3$[30] as compared with ≈130 mol% of Ti in $SrTiO_3$ in the current study) and the eventual formation of a layered, Ti-rich phase with nominal chemical formula $Sr_2Ti_7O_{14}$. Scanning transmission electron microscopy (STEM)-based studies map out the structure and valence state of this phase, first-principles

S. Lee, Dr. A. R. Damodaran, Dr. Z. Chen, Prof. L. W. Martin
Department of Materials Science and Engineering
University of California
Berkeley, Berkeley, California 94720, USA
E-mail: lwmartin@berkeley.edu
Dr. P. Gorai, N. Ferdous, Prof. E. Ertekin
Department of Mechanical Science and Engineering
University of Illinois
Urbana-Champaign, Urbana, Illinois 61801, USA
N. Oh, Dr. J.-H. Kwon, Dr. A. Shah, Dr. E. Breckenfeld, Dr. R. V. K. Mangalam, Prof. P. V. Braun, Prof. M. Shim, Prof. J.-M. Zuo
Department of Materials Science and Engineering
and Materials Research Laboratory
University of Illinois
Urbana-Champaign, Urbana, Illinois 61801, USA
Dr. J. A. Moyer, Prof. P. Schiffer
Department of Physics
University of Illinois
Urbana-Champaign, Urbana, Illinois 61801, USA

DOI: 10.1002/adma.201403602

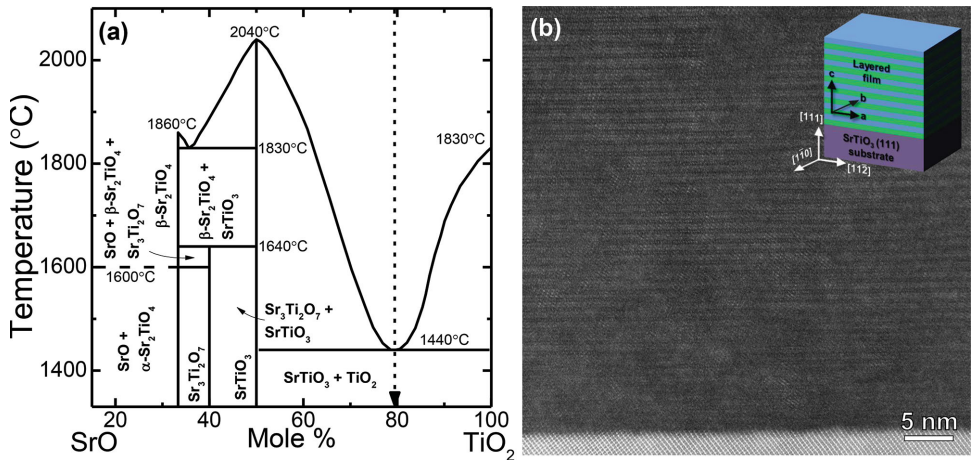

Figure 1. Self-assembled, layered eutectic $SrTiO_3$–TiO_2 film. a) Equilibrium eutectic phase diagram of SrO–TiO_2 system (Adapted with permission.[26] Copyright 1969, American Ceramic Society. Printed with permission of the American Ceramic Society (www.ceramics.org).). b) HAADF-STEM image of the resulting film of eutectic composition (21 mol% SrO/79 mol% TiO_2) grown on a $SrTiO_3$ (111) substrate. Inset shows alignment of the structure.

approaches explore the phase stability and electronic properties, and studies of the dielectric, optical, thermal, and magnetic properties reveal diminished dielectric permittivity (and low dielectric loss), an enhanced bandgap, glass-like thermal conductivity, and the potential for 2D anti-ferromagnetism.

In the equilibrium phase diagram (**Figure 1**a),[26] the eutectic composition for the $SrTiO_3$–TiO_2 system is located at 21 mol% SrO/79 mol% TiO_2. Films of the $SrTiO_3$–TiO_2 system were grown on $SrTiO_3$ (001), (110), and (111) substrates via pulsed-laser deposition from targets of the following compositions (where the first and second numbers refer to the mole percentage of SrO and TiO_2, respectively): 43:57, 33:67, 30:70, 25:75, 23:77, 21:79, 17:83, 10:90, and 0:100. Details of the growth process are provided in the Supporting Information. X-ray diffraction studies of all films (focusing on ≈100 nm thick films on $SrTiO_3$ (111) substrates) reveal only a single set of diffraction peaks and no evidence of phase separation or multiple phases (Figure S1, Supporting Information). Atomic-force microscopy studies reveal no evidence of phase separation with the surface remaining relatively smooth across all compositions (Figure S2, Supporting Information). Only upon in-depth cross-sectional high-angle annular dark-field (HAADF)-STEM imaging of the atomic structure of the films did clear differences emerge (see Figure S3, Supporting Information for details) and only when we reach the eutectic composition of 21 mol% SrO/79 mol% TiO_2 does the STEM imaging reveal the presence of an unexpected layered phase with an out-of-plane periodicity of ≈0.91 nm (Figure 1b). Such a layered phase was observed on (111)-oriented versions of $SrTiO_3$, $(LaAlO_3)_{0.3}$–$(Sr_2AlTaO_6)_{0.7}$ (LSAT), $LaAlO_3$, and Nb-doped $SrTiO_3$ substrates, but not on (001)- and (110)-oriented substrates (where complex and disordered structures are observed, Figure S3, Supporting Information).

High-resolution HAADF-STEM imaging (**Figure 2**a) and nano-area electron diffraction (NAED) (Figure 2b) were completed to assess the atomic structure of the phase (see Supporting Information for details). Both the STEM imaging and the NAED patterns reveal a periodicity of ≈0.91 nm along the out-of-plane direction (ca. 4 times longer than that of the $SrTiO_3$ {111} d-spacing). Along the in-plane direction, first- and second-order diffraction peaks (Figure 2b) reveal periodicities of ≈0.487 and ≈0.243 nm that correspond to Sr–Sr and Sr–O interatomic spacings, respectively. Comparison with the $SrTiO_3$ substrate (inset, Figure 2a,b) reveals that the layered phase is composed of layers with local coordination akin to that in $SrTiO_3$ that are separated by a monolayer of periodically aligned Ti- and O-ions (that exhibit reduced Z-contrast and are consistent with the highly Ti-rich nature of the film composition).

Average structural information about the layered phase was obtained using on-axis (about the 222-diffraction peak of the substrate) and off-axis (about the 113- and 042-diffraction peaks of the substrate) X-ray reciprocal space mapping (RSM) studies (Figure 2c–e). Here, we index the film assuming that the *a*, *b*, and *c* lattice parameters are parallel to the $[11\bar{2}]$, $[1\bar{1}0]$, and [111] of the substrate, respectively. The order of the diffraction condition is determined by comparison to the measured periodicities from the STEM imaging and NAED patterns. On-axis RSM studies (Figure 2c) show the presence of a film peak (indexed as the 008-diffraction condition) that reveals an out-of-plane lattice spacing $c \approx 0.915$ nm (commensurate with the 0.91 nm obtained from the STEM and NAED analysis). Off-axis RSM studies about the 042-diffraction condition of the substrate (Figure 2d) show the presence of a film peak indexed to be the 048-diffraction condition that enables calculation of the in-plane spacing $b \approx 0.569$ nm (≈3.1% expanded as compared with the substrate in the same direction). Off-axis RSM studies about the 113-diffraction condition of the substrate (Figure 2e) reveal the presence of a set of film peaks indexed to be the $\bar{4}07$- and $\bar{4}06$-diffraction conditions that enables calculation of the in-plane lattice spacing $a \approx 0.987$ nm (≈3.1% expanded as compared with the substrate lattice spacing in the same direction). ϕ-scans about the 042- and 048-diffraction conditions of the substrate and film (Figure 2f), respectively, reveal the epitaxial relationship to be $[100]_f//[11\bar{2}]_s$ and $[010]_f//[\bar{1}10]_s$ and, from STEM/NAED, the out-of-plane $[001]_f$ is found to be tilted by ≈10.2° from the $[111]_s$ (where f and s refer to film and substrate, respectively). In summary, the unit cell of the layered

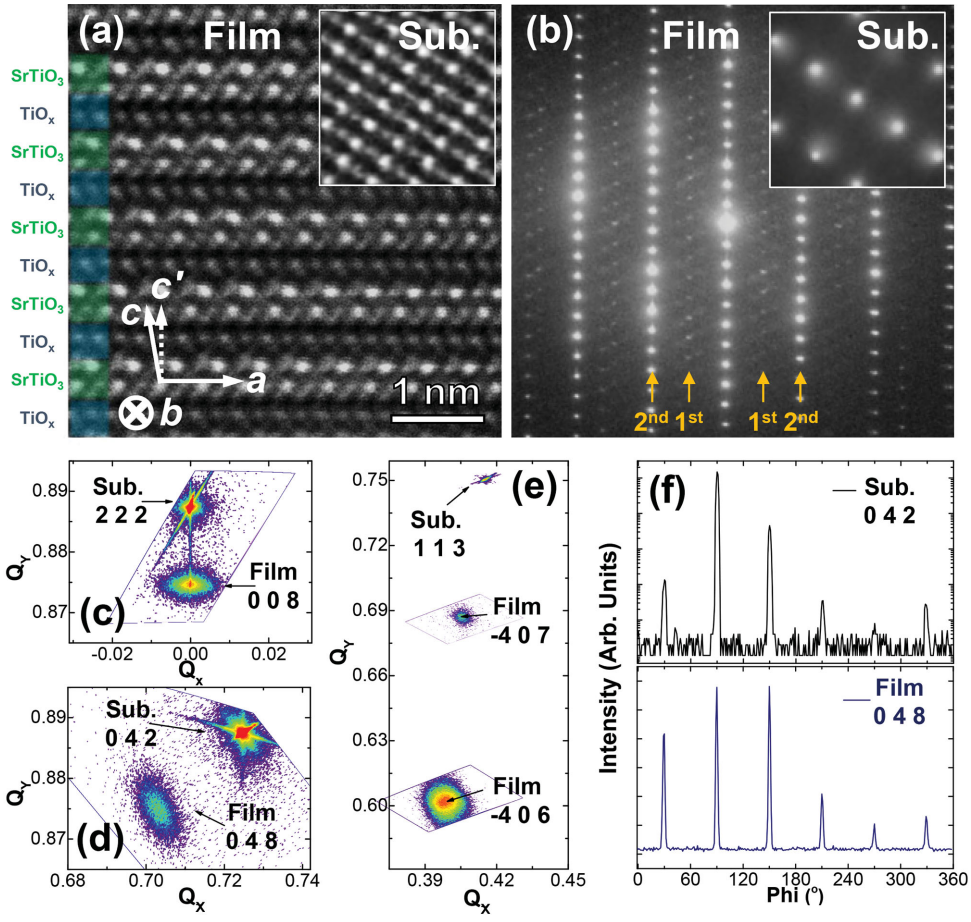

Figure 2. Structural characterization of the novel, layered phase. a) HAADF-STEM image after smoothing process (along the [1$\bar{1}$0] zone axis of the substrate) of the novel, layered phase. Inset shows a corresponding image along the same zone axis for the $SrTiO_3$ substrate. b) NAED pattern from the novel, layered phase. Inset shows a corresponding NAED pattern along the same zone axis for the $SrTiO_3$ substrate. RSM studies about the c) 222-, d) 042-, and e) 113-diffraction conditions of the substrate. f) ϕ-scans about the 042- and 048-diffraction conditions of the substrate and film, respectively, revealing the epitaxy of the film/substrate system.

phase is: $a = 0.987$ nm, $b = 0.569$ nm, $c = 0.929$ nm, $\alpha = \gamma = 90°$, and $\beta = 100.2°$. Note that this unit cell corresponds to two formula units (i.e., $Sr_4Ti_{14}O_{28}$) to fully encompass the complex symmetry of the system.

From the STEM imaging, it is possible to extract the atomic positions (of the cations) and to produce a model of the proposed structure. Although it is not possible to resolve all of the O-ions, the cation arrangement suggests that all Ti–O bonding should occur within octahedra (TiO_6) and that all O-sites are fully occupied to both compensate charge and coordination (a detailed discussion of the atomic model and simulated diffraction patterns is provided in Table S1 and Figure S4 and S5 in the Supporting Information). Based on the extracted interatomic distances, an atomic model can be constructed and the simulated diffraction pattern[31] for this initial model matches that obtained in the NAED studies well, suggesting a good initial understanding of the structure (Figure S5c, Supporting Information).

Disambiguation of the structure, however, requires additional steps. Briefly, the STEM imaging provides a projection of the atomic columns, but does not reveal the density or exact make-up of atoms in those columns. Thus, there were a number of potential candidate structures consistent with the image. We reiterate that no Ti-rich $SrTiO_3$ phases are reported within the vicinity of the eutectic composition in the equilibrium phase diagram. Although not reported on the equilibrium phase diagram, two Ti-rich phases have been reported in the literature: $Sr_2Ti_5O_{12}$[32] (corresponding to 29 mol% SrO/71 mol% TiO_2) and $Sr_2Ti_6O_{13}$[33] (corresponding to 25 mol% SrO/75 mol% TiO_2). Both phases are known to exist only as minor phases, are thought to be metastable, and are off in composition (8 and 4 mol% deficient in TiO_2, respectively) from the eutectic composition studied herein. Nonetheless, we have considered the possibility that these phases (or a phase possessing these nominal chemical formulas and a structure commensurate with that observed here) could be the novel, layered phase. A detailed description of these candidate phases is provided (Figure S6, Supporting Information).

Differentiation of the potential structures for the layered phase is achieved by chemical analyses. First, from Rutherford backscattering spectrometry (Figure S7, Supporting Information) the Sr:Ti ratio for the films is determined to be ≈1:3.6 that matches (within the experimental error) the $Sr_2Ti_7O_{14}$ phase.

Thus, from the atomic-level imaging, X-ray diffraction, and chemical analyses, the novel, layered phase produced during the growth of the eutectic composition materials is determined to be a new phase – $Sr_2Ti_7O_{14}$. The proposed unit cell for this phase is highlighted by the presence of layers with local coordination akin to that in $SrTiO_3$ that are separated by a monolayer of periodically aligned Ti- and O-ions. We also note that in the unit cell of this structure that there are three types of octahedral bonding including two corner-, four edge-, and eight face-sharing octahedra (Figure S5b, Supporting Information). This specific complex and close-packed TiO_6 octahedra arrangement is not reported in any published TiO_x phase, but corner-, edge-, and face-sharing octahedra are all possible in TiO_x systems. The appropriate charge balance of this structure could be achieved (theoretically, assuming nearly complete oxidation) with three possible combinations of Ti^{2+}:Ti^{3+}:Ti^{4+} species occurring in ratios of 2:0:5, 1:2:4, and 0:4:3. Previous studies suggest that face-sharing octahedra in Ti-based systems require the presence of Ti^{3+}[34] and since eight of the total 14 octahedra in the unit cell are face-sharing, we expect that Ti^{3+} must populate the majority of the Ti-sites, suggesting that the structure should possess a 0:4:3 ratio of Ti^{2+}:Ti^{3+}:Ti^{4+}.

The average valence state of Ti in $Sr_2Ti_7O_{14}$ was probed via STEM-based electron energy loss spectroscopy (EELS) studies of the Ti–$L_{2,3}$ and O–K edge spectra (**Figure 3**a). We observe a shift (to lower energies) and broadening of the Ti–$L_{2,3}$ peaks for the novel, layered phase as compared with the $SrTiO_3$ substrate consistent with what has been observed in oxygen-deficient $SrTiO_{3-\delta}$[35] and Ti_2O_3 (that possess only Ti^{3+} valence states)[36] thereby confirming the presence of a mixed Ti^{3+}/Ti^{4+} valence state. We also note that the intensity of the α peak from the O–K edge spectra is significantly diminished indicating that the Sr–O bonding contributes less to the spectra[37] which is, again, consistent with $Sr_2Ti_7O_{14}$ (especially the TiO_x inter-layers) possessing less Sr–O bonding compared with $SrTiO_3$.

Armed with this detailed structural and chemical data, we further explored the structure and stability of the $Sr_2Ti_7O_{14}$ phase via density functional theory (DFT) using hybrid functionals (see Supporting Information for details). Considering the possibility of several valence states for the Ti-ions within the structure, it is possible that the TiO_6 octahedra may be susceptible to energetically favorable internal distortions. Small perturbations of the TiO_6 octahedra may not be resolvable via experiment alone and we used the DFT approaches to assess the lowest energy structure of the $Sr_2Ti_7O_{14}$ phase. The simulations reveal that the structure is locally stable, and confirm the presence of slight octahedral distortions, for which we find an energy recovery of ≈3.4 eV per unit cell in comparison to the undistorted structure. This is a reasonably large energy recovery in comparison to the atomization energy, which we find to be ≈196 eV per unit cell. Several distinct distortions are present, corresponding to the various Ti^{3+} and Ti^{4+} environments for the octahedra. A schematic illustrating the lowest-energy structure is provided (Figure 3b,c). From this experimentally and DFT-optimized structure, we can thus compare the experimentally observed atomic structure (Figure 3d) to a simulated Z-contrast STEM image (Figure 3e), as well as a simulated selective area diffraction pattern (Figure 3f) to the actual NAED pattern. This comparison shows excellent and nearly ideal matching (including matched modulation of the intensity across the diffraction pattern); thereby confirming the extracted and optimized structure is representative of the real structure of the material.

Based on the structural analysis that suggests a new structure and phase, it is important to understand the mechanism for and nature of the evolution of this exotic phase. Clearly the structure that is formed deviates, somewhat dramatically, from the traditional eutectic system from which it was grown, and thus it warrants comparison with other exotic structures observed in materials – namely crystallographic shear structures (CSS). CSS can be considered as an example of so-called non-conservative defect structures – or defect structures that change the composition of the parent material – and have been found in a range of materials.[38–42] In transition metal oxides,

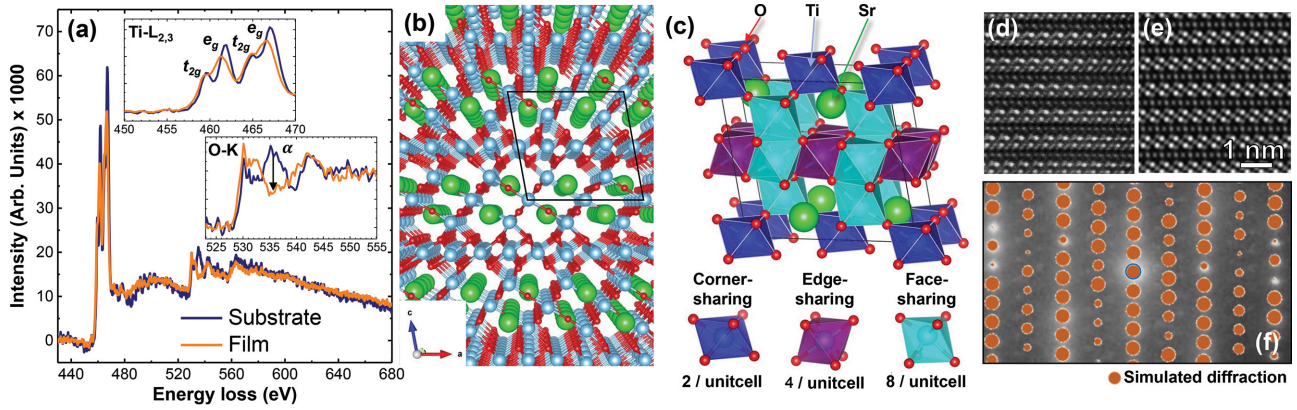

Figure 3. Atomic models and spectroscopy of the novel, layered phase. a) EELS profile from the novel, layered phase (orange) and $SrTiO_3$ substrate (blue) revealing the presence of a mixture of Ti^{3+}/Ti^{4+} in the former. Schematic illustrations of b) multiple unit cells (along the $[1\bar{1}0]$) and c) a 3D view of a single unit cell of the proposed (experimentally and DFT-optimized) structure for $Sr_2Ti_7O_{14}$ revealing the various types of TiO_6 octahedra bonding including corner- (blue), edge- (violet), and face-sharing (cyan). d) Smoothed Z-contrast STEM image of the novel layered phase. e) Simulated Z-contrast STEM image of the same area of the novel layered phase confirming excellent matching of the extracted structure. f) Simulated diffraction pattern for the model structure overlaid on the top of the NAED diffraction pattern revealing excellent matching. The blue circle marks the 000 diffraction condition.

special non-conservative defect structures occur whereby a reduction of the oxygen content results in a disruption of the underlying structural framework whence the structure is effectively cleaved, a fraction of the oxygen ions are removed, and the structure is placed back together, now sheared (or shifted) with respect to one another thereby creating a so-called crystallographic shear plane.[38,43] While early work on CSS focused on binary oxide materials, more recent work has explored CSS in ternary, anion-deficient perovskites[42,44–47] and others have gone on to extend the idea to cation-excess systems such as the RP homologous series.[48–50] In a similar spirit, it is possible to discuss $Sr_2Ti_7O_{14}$ within the confines of CSS. Assuming that the parent material is in fact $SrTiO_3$ and noting that the full unit cell for our system has been determined to be $Sr_4Ti_{14}O_{28}$, we would then want to compare this to 14 unit cells of the parent $SrTiO_3$ (i.e., $Sr_{14}Ti_{14}O_{42}$). $Sr_2Ti_7O_{14}$ could be produced upon the removal of 10 Sr- and 14 O-ions from the 14 unit cells of $SrTiO_3$ (or 0.71 Sr and 0.33 O per unit cell of $SrTiO_3$). The Sr and O are preferentially removed from (111) in the structure (producing layers of TiO_x with no Sr atoms) and the remaining perovskite layers are sheared by ½[112].

Such a comparison with CSS may provide an alternative way of thinking about this system, but is important to point out a number of ways that the $Sr_2Ti_7O_{14}$ differs from traditional CSS systems. First, as noted from the analysis above, $Sr_2Ti_7O_{14}$ is a fully oxidized system (i.e., with the exception of a small, equilibrium density of oxygen vacancies common to all oxide materials, all available oxygen sites in the structure are fully occupied) like in the case of the RP phases. In $Sr_2Ti_7O_{14}$ the mixed Ti^{3+} and Ti^{4+} valence state originates from the coordination environment of the Ti-ions in the TiO_x-layers, not from large-scale oxygen deficiency. This is different from the vast majority of work on CSS that has focused on significantly anion-deficient systems. Second, the nature of the non-stoichiometry is both opposite to and vastly larger in magnitude in $Sr_2Ti_7O_{14}$ than in previously examined systems. In the RP systems, for instance, there is *A*-site excess and in the worst case that excess is only 2:1 *A*:*B* ratio whereas in $Sr_2Ti_7O_{14}$ there is *B*-site excess with a much larger 2:7 *A*:*B* ratio. Finally, typical CSS systems lack long-range order to the CSS since there is a degenerate family of shear planes. This typically causes the material to possess complex rotations of the CSS giving rise to what some have called waves, hairpins, and Γ-shapes as in the case of the $A_nB_nO_{3n-2}$ homologous series of perovskite-based CSS.[42] In the $Sr_2Ti_7O_{14}$ phase, however, we have observed only one variant of the potential CSS that runs parallel to the growth plane of the film in a highly ordered, periodic fashion across the sample.

In the end, articulation of the structure within the parlance of CSS may help shed some light on the mechanism underlying the formation of this structure. Ultimately it appears to be an extreme type of CSS that is likely influenced by a number of factors. First, thin-film epitaxy and substrate orientation appear to play a critical role since growth of films simultaneously on $SrTiO_3$ (001), (110), and (111) substrates reveals that only the (111)-oriented substrates give rise to the $Sr_2Ti_7O_{14}$ phase. This likely arises from the fact that the TiO_x layers in the structure, which possess sixfold symmetry, would be difficult to form on the fourfold or twofold symmetric cubic and rectangular lattices of (001)- and (110)-oriented substrates (in other words, the (111) surface is the only orientation that can accommodate the CSS). Second, the film composition is found to be important since a deviation of only ≈3 mol% in TiO_2 composition can destroy the phase (Figure S3, Supporting Information). Finally, the kinetics of the growth process appear to play a role. Truly this is a non-equilibrium structure and the degree of order in the $Sr_2Ti_7O_{14}$ increases as the growth rate is reduced suggesting that the formation of the phase requires sufficient time for the diffusion/rearrangement of the constituent ions. The system is likely metastable in the sense that the $Sr_2Ti_7O_{14}$ was found to be stable at growth temperatures <850 °C, above which the film decomposes into two phases (rutile TiO_2 and $SrTiO_3$).

Having established the structure, we proceed to explore the electronic structure and physical properties of $Sr_2Ti_7O_{14}$ including optical absorption, dielectric permittivity and loss, thermal conductivity, and magnetism. Again, due to the presence of mixed-valence cations [Ti^{3+} ($3d^1$) and Ti^{4+} ($3d^0$)], special attention was given to probing the electronic structure and potential for spin ordering. In structures with face-, edge-, and corner-sharing octahedra, superexchange and direct exchange mechanisms compete with each other and the prevailing spin configuration is determined by a competition between different exchange interactions that are affected by electron occupancy of orbitals, bond angles, and cation–cation separation.[51–53] From inspection of the crystal structure, two spin configurations are possible. In the first, direct exchange interactions within both pairs of Ti-ions participating in face-sharing octahedra drive localization of the excess electrons. In this configuration, a direct exchange interaction *J* is expected to be large within a pair of face-sharing octahedra, but weaker from one pair to the next. In the second, the Ti-ions (in the TiO_x plane) participating in edge-sharing octahedra carry the excess electrons and superexchange mechanisms support a 2D ordered spin configuration.

Conventional DFT simulations[54] predict that the structure is not spin-polarized and, although there is a large gap between the nominal valence and conduction bands, the Fermi level is located above the conduction band edge and the system is predicted to be metallic (which it is not). Additionally, rather than distinct Ti^{3+}-and Ti^{4+}-ions, the extra electrons are shared equally amongst all Ti-ions (in the TiO_x plane) in a metallic state. Moving to hybrid DFT calculations, which we expect to be more accurate in this case, we are able to assess the possibility of charge and spin ordering. For a standard choice of hybrid parameters,[55] we predict that an anti-ferromagnetic checkerboard-like spin configuration, in which the excess electrons are localized on the Ti-ions within the TiO_x plane (**Figure 4**a), is more stable than the non-magnetic one by ≈0.2 eV/unit cell. Examination of the distribution of up- and down-spin electron density within the TiO_x plane (Figure 4b) shows the nature of the anti-ferromagnetic order and how the oxygen ions along the octahedral shared edges mediate the anti-ferromagnetic Ti configuration via superexchange, indicating that the second scenario considered above prevails. It should also be noted, that the spin-down electron distributions are observed to extend asymmetrically out of the plane toward the neighboring Ti atoms across the shared octahedral face, suggesting that mild elements of the first scenario (a ferromagnetic coupling across

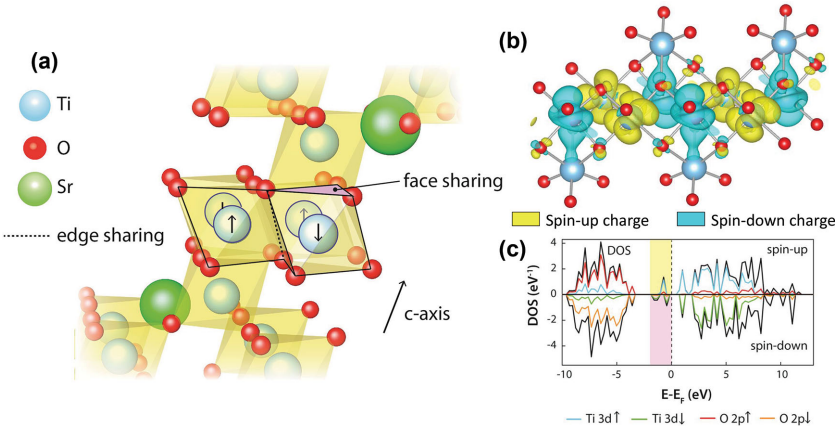

Figure 4. Spin configuration, orbital charge density, and electronic density of states of the novel, layered phase. Schematic illustration of a) the proposed spin configuration in which the edge-sharing, planar TiO_6 octahedra exhibit a $3d^1$ electron valence and a checkerboard anti-ferromagnetic spin configuration and b) the charge density of the orbitals corresponding to this configuration according to hybrid DFT calculations, showing the occupation of orbitals to minimize electron overlap. c) Corresponding electronic density of states for the system.

face sharing octahedra due to direct exchange) are also present, but weaker than the anti-ferromagnetic order within the plane.

Finally, the electronic density of states (Figure 4c) reveals three distinct sets of states are present in the vicinity of the Fermi energy. The lower set of states (nominally the valence band), exhibits an oxygen 2*p* character while the intermediate and upper (nominally conduction band) exhibit a Ti 3*d* character. The intermediate states are highly localized to the edge-sharing Ti atoms in the TiO_x plane and likely are states offset from the conduction bands, stabilized in part by exchange interactions leading to the anti-ferromagnetic configuration.[56] The primary gap is calculated to be 3.7–3.8 eV.

Subsequent experimental study confirms many of these observations. Magnetic measurements of the sample cooled from 550 K in a magnetic field and in zero field reveal no ferromagnetic ordering either in- or out-of-the-plane of the film from 4 to 550 K, but a broad peak in the magnetic susceptibility was observed in both field cooled and zero field cooled measurements around 400 K, which could be indicative of anti-ferromagnetic ordering in the material and is consistent with the predictions of anti-ferromagnetic order from the hybrid DFT studies. Transmittance and reflectance studies of $Sr_2Ti_7O_{14}/LaAlO_3$ (111) heterostructures also confirm the predictions of the hybrid DFT studies. A linear fit of $\alpha h\upsilon^2$ (where α is the absorption coefficient, h is Planck constant, and υ is the frequency of photon) as a function of the photon energy ($h\upsilon$) (**Figure 5**a) reveals a direct bandgap for $Sr_2Ti_7O_{14}$ of ≈3.87 eV. The decreased transmittance in $Sr_2Ti_7O_{14}$ between 360 and 660 nm is due to the $LaAlO_3$ substrate with complex twin structures that reflect the visible light diffusively and decreases the transmittance. See the Supporting Information for details of these measurements.

Likewise, probes of electronic conduction reveal a highly insulating material (albeit with some anisotropy). When measured in the out-of-plane geometry, 100 nm thick films revealed low leakage current densities of <0.01 μA cm^{-2} even under applied electric fields in excess of 200 kV cm^{-1} while measurements in the in-plane geometry revealed leakage currents at least 10^2-times larger, but still indicative of an insulating material (Figure S8, Supporting Information). Such observations are consistent with what might be expected based on the highly anisotropic structure, which could limit conduction out-of-the-plane of the film and based on what has been observed mixed Ti^{3+}/Ti^{4+} TiO_x compounds where the conductivity can be larger than in purely Ti^{4+} systems.[57] Subsequent probes of the out-of-plane dielectric permittivity (ε_r) and loss tangent of $Sr_2Ti_7O_{14}$/Nb-doped $SrTiO_3$ (111) heterostructures at room temperature as a function of frequency have also been completed (Figure 5b). The dielectric permittivity of the $Sr_2Ti_7O_{14}$ films was found to be essentially frequency-independent with a value of 48 with low loss tangents (0.002 at 10 kHz) in the frequency range 1–100 kHz. This low dielectric permittivity may be expected considering that the $Sr_2Ti_7O_{14}$ phase consists of $SrTiO_3$-like layers ($\varepsilon_r \approx 300$) and layers of face-sharing octahedra TiO_x layers (which are structurally similar to Ti_2O_3 that has a $\varepsilon_r \approx 45$)[58] that effectively produce a nanoscale, layered dielectric.

Lastly, the thermal conductivity (κ) of the $Sr_2Ti_7O_{14}$ films was measured in the film-normal direction by time-domain thermoreflectance (TDTR)[59] (see Figure S9, Supporting Information for details). We note that the thermal conductivity of the $Sr_2Ti_7O_{14}$ films shows a significantly lower value of $\kappa \approx 1.3$ W m-K^{-1} compared with parent phases $SrTiO_3$ and TiO_2 that range between 8.8 and 11.2 W m^{-1} K^{-1}[60,61] whereas the speed of sound of the layered film remains essentially the same as the parent phases. Previously, low κ has been observed in artificially synthesized $SrTiO_3$-superlattice systems ($\kappa \geq 2.8$ W m^{-1} K^{-1} for $(SrTiO_3)_m/(CaTiO_3)_n$ and $\kappa \geq 1.8$ W m^{-1} K^{-1} for $(SrTiO_3)_m/(BaTiO_3)_n$ superlattices)[62] and in $Sr_{n+1}Ti_nO_{3n+1}$ RP-phases ($\kappa \geq 4.5$ W m^{-1} K^{-1}),[63] but not as low as that observed in the $Sr_2Ti_7O_{14}$ films. We hypothesize that the glass-like thermal conductivity arises from two main contributions: i) significant phonon scattering at the boundaries between $SrTiO_3$-like and TiO_x layers in this phase and ii) a low contribution of electronic thermal conductivity from low free electron concentration. This is not surprising considering that $Sr_2Ti_7O_{14}$ has a periodic spacing of 0.91 nm in the out-of-plane direction (excellent for scattering portions of the heat carrying phonons) and that the electrical conductivity is extremely low as we observed from the leakage experiment. The ability to produce highly ordered layered structures with subnanometer length-scales could open up many opportunities for low thermal transport applications.

In conclusion, we have synthesized a new phase $Sr_2Ti_7O_{14}$ that self-assembled into a highly ordered, layered structure that consists of layers with local order akin to that of $SrTiO_3$ separated by close-packed, TiO_x layers by combining non-equilibrium growth techniques, thin-film epitaxy, and a system with an innate chemical/structural instability. We observe that the layered $Sr_2Ti_7O_{14}$ phase is realized only at the eutectic composition of the $SrTiO_3$–TiO_2 system, when growth takes place on

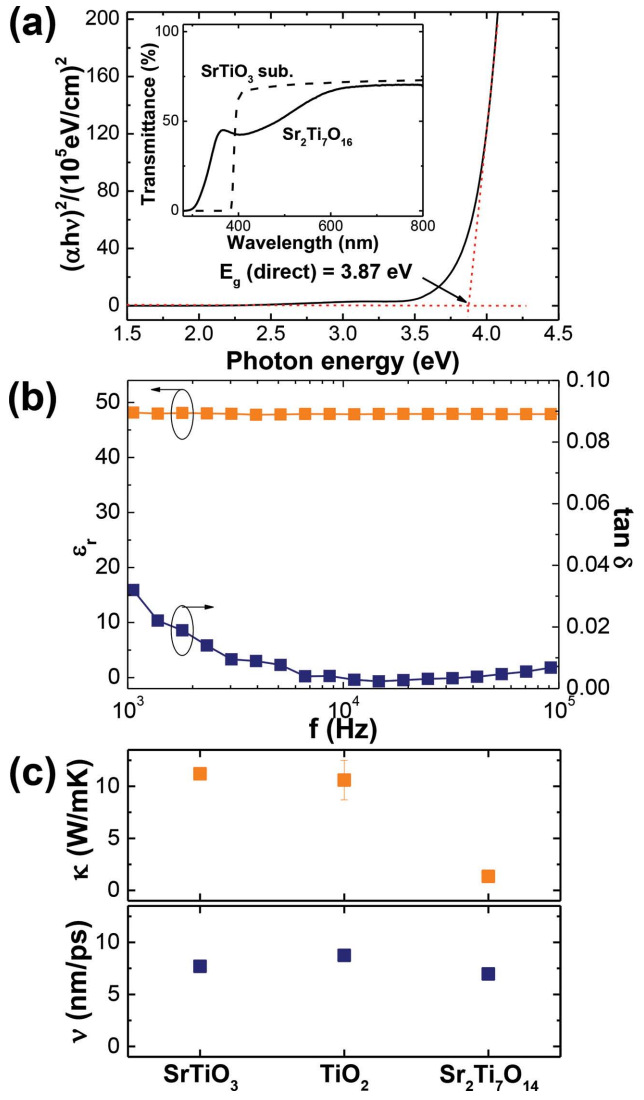

Figure 5. Optical, dielectric, and thermal properties of the novel, layered phase. a) The dependence of $\alpha h\nu^2$ on photon energy ($h\nu$) and (inset) transmittance of the $Sr_2Ti_7O_{14}$ phase. b) Dielectric permittivity (ε_r) and loss tangent (tanδ) of the $Sr_2Ti_7O_{14}$ phase measured at 10 mV of ac voltage bias with no dc bias as a function of frequency. c) Thermal conductivity (κ, top) and speed of sound (υ, bottom) for $SrTiO_3$, TiO_2, and $Sr_2Ti_7O_{14}$ as measured by TDTR.

(111)-oriented perovskite substrates, and when the kinetics of the growth process are appropriately controlled. It should be noted, however, that although the phase is found to form at the eutectic composition, the role of the innate eutectic tendency of this system in stabilizing this layered phase is not fully understood at this point and is clearly a matter for future studies in other systems. In-depth X-ray and electron diffraction studies and imaging have allowed for the precise identification of the structure and unit cell of this phase. Subsequent chemical and spectroscopic studies were used to confirm these studies. The $Sr_2Ti_7O_{14}$ phase possesses properties that are unique from the parent $SrTiO_3$ and TiO_2 phases including a larger optical bandgap of 3.87 eV, reduced dielectric constant of 48, low dielectric loss, and a glass-like thermal conductivity of 1.3 W m^{-1} K^{-1}. This unique approach to the formation of high-ordered layered materials could represent a new modality to achieve novel states of matter in other systems possessing similar chemical/structural instabilities and can provide new insights into the design of hierarchical structures by self-assembly.

Supporting Information

Supporting Information is available from the Wiley Online Library or from the author.

Acknowledgements

S.L., Z.C., P.V.B., and L.W.M. acknowledge the support of the Air Force Office of the Scientific Research under grant FA9550–12–1–0471. A.R.D. acknowledges support from the Army Research Office under grant W911NF-14–1–0104. E.B. acknowledges support from the National Science Foundation under grant DMR-1124696. P.G, N.F, and E.E. acknowledge support from the Strategic Research Initiatives Program of the College of Engineering at the University of Illinois at Urbana-Champaign. N.O. and M.S. acknowledge support from the National Science Foundation under grant CHE-1153081. The work was carried out, in part, in the Materials Research Laboratory Central Research Facilities, University of Illinois.

Received: August 7, 2014
Revised: October 20, 2014
Published online: December 18, 2014

[1] R. L. Ashbrook, *J. Am. Ceram. Soc.* **1977**, *60*, 428.
[2] V. S. Stubican, R. C. Brandt, *Annu. Rev. Mater. Sci.* **1981**, *11*, 267.
[3] Y. Waku, N. Nakagawa, T. Wakamoto, H. Ohtsubo, K. Shimizu, Y. Kohtoku, *Nature* **1997**, *389*, 49.
[4] J. L. Llorca, V. M. Orera, *Prog. Mater. Sci.* **2006**, *51*, 711.
[5] H. Zheng, J. Wang, S. E. Lofland, Z. Ma, L. Mohaddes-Ardabili, T. Zhao, L. Salamanca-Riba, S. R. Shinde, S. B. Ogale, F. Bai, D. Viehland, Y. Jia, D. G. Schlom, M. Wuttig, A. Roytburd, R. Ramesh, *Science* **2004**, *303*, 661.
[6] B. S. Guiton, P. K. Davies, *Nat. Mater.* **2007**, *6*, 586.
[7] J. L. MacManus-Driscoll, *Adv. Funct. Mater.* **2010**, *20*, 2035.
[8] S. A. Harrington, J. Zhai, S. Denev, V. Gopalan, H. Wang, Z. Bi, S. A. T. Redfern, S.-H. Baek, C. W. Bark, C.-B. Eom, Q. Jia, M. E. Vickers, J. L. MacManus-Driscoll, *Nat. Nanotechnol.* **2011**, *6*, 491.
[9] W. Zhang, A. Chen, Z. Bi, Q. Jia, J. L. MacManus-Discoll, H. Wang, *Curr. Opin. Solid State Mater. Sci.* **2013**, *18*, 6.
[10] M. Muralidhar, N. Sakai, M. Nishiyama, M. Jira, T. Machi, *Appl. Phys. Lett.* **2003**, *82*, 943.
[11] L. Mohaddes-Ardabili, H. Zheng, S. B. Ogale, B. Hannoyer, W. Tian, J. Wang, S. E. Lofland, S. R. Shinde, T. Zhao, Y. Jia, L. Salamanca-Riba, D. G. Schlom, M. Wuttig, R. Ramesh, *Nat. Mater.* **2004**, *3*, 533.
[12] J. L. MacManus-Driscoll, P. Zerrer, H. Wang, H. Yang, J. Yoon, A. Fouchet, R. Yu, M. G. Blamire, Q. Jia, *Nat. Mater.* **2008**, *7*, 314.
[13] Y. Lu, C. Wang, Y. Gao, R. Shi, X. Liu, Y. Wang, *Phys. Rev. Lett.* **2012**, *109*, 086101.
[14] M. Parlier, R. Valle, L. Perrière, S. Lartigue-Korinek, L. Mazerolles, *J. Aerosp. Lab.* **2011**, AL03.
[15] A. Revcolevschi, G. Dhalenne, *Adv. Mater.* **1993**, *5*, 657.
[16] D. A. Pawlak, S. Turczynski, M. Gajc, K. Kolodziejak, R. Diduszko, K. Rozniatowski, J. Smalc, I. Vendik, *Adv. Funct. Mater.* **2010**, *20*, 1116.

[17] R. M. White, J. M. Kunkle, A. V. Polotai, E. C. Dickey, *J. Eur. Ceram. Soc.* **2011**, *31*, 1227.
[18] H. M. Christen, G. Eres, *J. Phys.: Condens. Matter* **2008**, *20*, 264005.
[19] D. G. Schlom, L.-Q. Chen, X. Pan, A. Schmehl, M. A. Zurbuchen, *J. Am. Ceram. Soc.* **2008**, *91*, 2429.
[20] L. W. Martin, Q. Zhan, Y. Suzuki, R. Ramesh, M. Chi, N. Browning, T. Mizoguchi, J. Kreisel, *Appl. Phys. Lett.* **2007**, *90*, 062903.
[21] R. J. Zeches, M. D. Rossell, J. X. Zhang, A. J. Hatt, Q. He, C.-H. Yang, A. Kumar, C. H. Wang, A. Melville, C. Adamo, G. Sheng, Y.-H. Chu, J. F. Ihlefeld, R. Erni, C. Ederer, V. Gopalan, L.-Q. Chen, D. G. Schlom, N. A. Spaldin, L. W. Martin, R. Ramesh, *Science* **2009**, *326*, 977.
[22] M. Dawber, N. Stucki, C. Lichtensteiger, S. Gariglio, P. Ghosez, J.-M. Triscone, *Adv. Mater.* **2007**, *19*, 4153.
[23] E. Bousquet, M. Dawber, N. Stucki, C. Lichtensteiger, P. Hermet, S. Gariglio, J.-M. Triscone, P. Ghosez, *Nature* **2008**, *452*, 732.
[24] J. Chakhalian, A. J. Millis, J. Rondinelli, *Nat. Mater.* **2012**, *11*, 92.
[25] H. Y. Hwang, Y. Iwasa, M. Kawasaki, B. Keimer, N. Nagaosa, Y. Tokura, *Nat. Mater.* **2012**, *11*, 103.
[26] M. K. Reser, *Phase Diagrams for Ceramists*, American Ceramic Society, Columbus, OH, USA **1969**.
[27] J. H. Haeni, C. D. Theis, D. G. Schlom, W. Tian, X. Q. Pan, H. Chang, I. Takeuchi, X.-D. Xiang, *Appl. Phys. Lett.* **2001**, *78*, 3292.
[28] C.-H. Lee, N. D. Orloff, T. Birol, Y. Zhu, V. Goian, E. Rocas, R. Haislmaier, E. Vlahos, J. A. Mundy, L. F. Kourkoutis, Y. Nie, M. D. Biegalski, J. Zhang, M. Bernhagen, N. A. Benedek, Y. Kim, J. D. Brock, R. Uecker, X. X. Xi, V. Gopalan, D. Nuzhnyy, S. Kamba, D. A. Muller, I. Takeuchi, J. C. Booth, C. J. Fennie, D. G. Schlom, *Nature* **2013**, *502*, 532.
[29] T. Suzuki, Y. Nishi, M. Fujimoto, *Philos. Mag. A* **2000**, *80*, 621.
[30] S. Witek, D. M. Smyth, *J. Am. Ceram. Soc.* **1984**, *67*, 372.
[31] J.-M. Zuo, J. C. Mabon, *Microsc. Microanal.* **2004**, *10*, S02.
[32] B. Peplinski, Th. Hübert, M. Willfahrt, U. Banach, *Mater. Sci. Forum* **1996**, *228*, 531.
[33] C. M. Liu, X. T. Zu, W. L. Zhou, *J. Phys. D: Appl. Phys.* **2007**, *40*, 7318.
[34] M. G. Vincent, K. Yvon, A. Grüttner, *Acta Crystallogr.* **1980**, *36*, 803.
[35] D. A. Muller, N. Nakagawa, A. Ohtomo, J. L. Grazul, H. Y. Hwang, *Nature* **2004**, *430*, 657.
[36] E. Stoyanov, F. Langenhorst, G. Steinle-Neumann, *Am. Mineral.* **2006**, *92*, 577.
[37] Z. Zhang, W. Sigle, M. Rühle, *Phys. Rev. B* **2002**, *66*, 094108.
[38] L. A. Bursill, B. G. Hyde, *Prog. Solid State Chem.* **1972**, *7*, 177.
[39] J. C. Ruiz-Morales, J. Canales-Vazquez, C. Savaniu, D. Marrero-Lopez, W. Zhou, J. T. S. Irvine, *Nature* **2006**, *439*, 568.
[40] G. Van Tendeloo, O. I. Lebedev, M. Hervieu, B. Raveau, *Rep. Prog. Phys.* **2004**, *67*, 1315.
[41] E. D. Sprecht, A. Goyal, J. Li, P. M. Martin, X. Li, M. W. Rupich, *Appl. Phys. Lett.* **2006**, *89*, 162510.
[42] M. Batuk, S. Turner, A. M. Abakumov, D. Batuk, J. Hadermann, G. Van Tendeloo, *Inorg. Chem.* **2014**, *53*, 2171.
[43] J. S. Anderson, J. M. Browne, A. K. Cheetham, R. Von Dreele, J. L. Hutchison, F. J. Lincoln, D. J. M. Bevan, J. Straehle, *Nature* **1973**, *243*, 81.
[44] A. M. Abakumov, J. Hadermann, G. Van Tendeloo, E. V. Antipov, *J. Am. Chem. Soc.* **2008**, *91*, 1807.
[45] A. M. Abakumov, J. Hadermann, S. Bals, I. V. Nikolaev, E. V. Antipov, G. Van Tendeloo, *Angew. Chem. Int. Ed.* **2006**, *45*, 6697.
[46] A. M. Abakumov, J. Haderman, M. Batuk, H. D'Hondt, O. A. Tyablikov, M. g. Rozova, K. V. Pokholok, D. S. Filimonov, D. V. Sheptyakov, A. A. Tsirlin, D. Niermann, J. Hemberger, G. Van Tendeloo, E. V. Antipov, *Inorg. Chem.* **2010**, *49*, 9508.
[47] J. Hadermann, A. M. Abakumov, I. V. Nikolaev, E. V. Antipov, G. Van Tendeloo, *Solid State Sci.* **2008**, *10*, 382.
[48] R. J. D. Tilley, *J. Solid State Chem.* **1977**, *21*, 293.
[49] M. A. McCoy, R. W. Grimes, W. E. Lee, *Philos. Mag. A* **1997**, *75*, 833.
[50] A. P. Tomsia, A. M. Glaeser, *Ceramic Microstructures: Control at the Atomic Level*, Plenum Press, New York **1998**.
[51] J. Kanamori, *Prog. Theor. Phys.* **1957**, *17*, 177.
[52] J. Kanamori, *Prog. Theor. Phys.* **1957**, *17*, 197.
[53] J. B. Goodenough, *J. Phys. Chem. Solids* **1958**, *6*, 287.
[54] J. Perdew, K. Burke, M. Ernzerhof, *Phys. Rev. Lett.* **1996**, *77*, 3865.
[55] A. V. Krukau, O. A. Vydrov, A. F. Izmaylov, G. E. Scuseria, *J. Chem. Phys.* **2006**, *125*, 224106.
[56] P. Gori, N. Ferdous, E. Ertekin, unpublished.
[57] F. J. Morin, *Phys. Rev. Lett.* **1959**, *3*, 34.
[58] G. Lucovsky, R. J. Sladek, J. W. Allen, *Phys. Rev. B* **1977**, *16*, 5452.
[59] D. G. Cahill, W. K. Ford, K. E. Goodson, G. D. Mahan, A. Majumdar, H. J. Maris, R. Merlin, S. R. Phillpot, *J. Appl. Phys.* **2003**, *93*, 793.
[60] E. Breckenfeld, R. Wilson, J. Karthik, A. R. Damodaran, D. G. Cahill, L. W. Martin, *Chem. Mater.* **2012**, *24*, 331.
[61] D. J. Kim, D. S. Kim, S. Cho, S. W. Kim, S. H. Lee, J. C. Kim, *Int. J. Thermophys.* **2004**, *25*, 281.
[62] J. Ravichandran, A. K. Yadav, R. Cheaito, P. B. Rossen, A. Soukiassian, S. J. Suresha, J. C. Duda, B. M. Foley, C.-H. Lee, Y. Zhu, A. W. Lichtenberger, J. E. Moore, D. A. Muller, D. G. Schlom, P. E. Hopkins, A. Majumdar, R. Ramesh, M. A. Zurbuchen, *Nat. Mater.* **2014**, *13*, 168.
[63] K. H. Lee, S. W. Kim, H. Ohta, K. Koumoto, *J. Appl. Phys.* **2006**, *100*, 063717.